

# Influence of hyperon-hyperon interaction on the properties of neutron stars

R. M. Aguirre \*

*Departamento de Física, Facultad de Ciencias Exactas,  
Universidad Nacional de La Plata,  
and IFLP, UNLP-CONICET, C.C. 67 (1900) La Plata, Argentina.*

## Abstract

The properties of neutron stars are studied in a composite model of the strong interaction. In the regime of low to medium baryonic densities a covariant hadronic model is adopted which includes an exclusive channel for the hyperon-hyperon interaction mediated by hidden strangeness mesons, which in turn couple to other mesons through polynomial vertices. The new coupling constants are subject to phenomenological constraints. The presence of free quarks in the core of the star is considered by using the Nambu-Jona Lasinio model supplemented with a vector interaction. The deconfinement process is described by a continuous coexistence of phases. Several structure parameters of neutron stars, such as mass-radius relation, moment of inertia, tidal deformability, and the propagation of non-radial f and g-modes within the relativistic Cowling approximation are studied. The predictions of the model are in good agreement with recent observational data, in particular the maximum inertial mass is greater than the observational lower limit of two solar masses.

## 1 Introduction

The astronomical observation of compact stars has become the most promising source of evidence for the study of matter at extreme densities and low temperatures. It is expected that the different manifestations of the interacting matter will leave its imprint in specific aspects of the structure and dynamics of these stars. From the theoretical point of view, the study of neutron stars is an excellent opportunity to try a unified theoretical description covering the many facets of the strong interaction in combination with gravitation, and to contrast predictions with empirical results.

The field has been a subject of permanent growing and interest, and the accelerated advances in the observational techniques has concentrated multiplied efforts in recent years. Thus a large amount of data has been acquired and is able for analysis. With the prospect of new and more precise measurements under an improved technology, it is expected that this trend will continue in the near future.

---

\*Email address: [aguirre@fisica.unlp.edu.ar](mailto:aguirre@fisica.unlp.edu.ar)

Some properties of the stellar structure are more transparent for understanding the microscopic behavior of the matter that compose it, and are taken as true guidelines to extract local information from the global experimental evidence. A few of them are highlighted in the following paragraphs.

The lowest upper bound for the inertial mass of a neutron star has been established around  $M_{\max} \simeq 2 M_{\odot}$  according to recent evidence [1, 2, 3]. Whereas it is not clear yet if the report [4] of a compact object with a mass  $M/M_{\odot} = 2.5 - 2.67$  corresponds to a black hole or to a neutron star. In the last case a serious questioning is posed against most of the descriptions of the strong interacting matter used at present [5]. In fact only a few microscopic models are able to reach such large value for the inertial mass. They commonly use the conventional nuclear degrees of freedom from the crust to the core of the star. The equation of state (EoS) of the dense matter becomes softer as other energetically favorable configurations are considered. The rise of the hyperon population [6, 7, 8], the emergence of resonances such as the  $\Delta$  isobar [9, 10, 11, 12, 13, 14], the meson condensates [15, 16, 17], the deconfinement phase transition [18], or the mixing with dark matter [19, 20, 21], are examples where the maximum mass is reduced due to the softening of the EoS.

The mass-radius relation has been inferred for the object PSR J0030+0451 [22] obtaining  $M = 1.34_{-0.16}^{+0.15} M_{\odot}$ ,  $R = 12.71_{-1.19}^{+1.14}$  km. For the case PSR J0740+6620 the results are  $M = 2.072_{-0.066}^{+0.067} M_{\odot}$ , and  $R = 12.39_{-0.98}^{+1.30}$  km [23]. Combining these and other experimental evidence the radius of the star with  $M/M_{\odot} = 1.4$  has been estimated within the range  $11.4 \text{ km} < R < 13.1 \text{ km}$  [24]. This result rules out some commonly used models, such as MS0 [25] and NL3 [26], which employ exclusively the low density nuclear degrees of freedom to reach the condition  $M_{\max} \geq 2.5 M_{\odot}$ . Although they would be admissible when combined with dark matter models to describe homogeneously admixed stars [27, 28].

The moment of inertia encodes valuable information about the organization of matter inside the star and can be related to the formation and evolution of double systems of compact objects [29]. There is great expectation for the measurement of the moment of inertia of one of the components of the pulsar binary system PSR J0737-3039 [30], which is particularly favorable for this purpose. Different procedures has been proposed to distinguish the underlying EoS, such as comparison with the prediction of specific models [31, 32, 33, 34], use of empirical universal relations [35], and statistical analysis [36].

Closely related to the measurement of the star masses and moments of inertia is the mutual deformation of a double star system due to gravitation. It has been proposed that tidal deformability, i.e. the quotient of the quadrupole deformation to the perturbing tidal field, is the relevant quantity to describe the gravitational wave phase emitted in the early steps of the collapse of a binary system [37]. Thus in the event GW170817 the masses of the pair has been determined either as  $1.36 < m_1/M_{\odot} < 1.60$  and  $1.16 < m_2/M_{\odot} < 1.37$  for the low spin regime, or  $1.36 < m_1/M_{\odot} < 2.26$  and  $0.86 < m_2/M_{\odot} < 1.36$  for higher angular momentum [38]. In addition an upper bound for the tidal deformability  $\Lambda_{1.4} \leq 970$  (800) of a neutron star with mass  $1.4 M_{\odot}$  was established for each of the regimes just mentioned. Further refinements [39] obtained the preferable values  $1.36 < m_1/M_{\odot} < 1.62$ ,  $1.15 < m_2/M_{\odot} < 1.36$ , and  $\Lambda_{1.4} = 190_{-120}^{+390}$ .

The propagation of nonradial oscillations inside a compact star is a longstanding issue [40, 41], which has gained renewed interest because of its relation with the gravitational waves and the recent first detection of such waves coming from the collapse of a binary system of neutron stars [38, 39, 42]. A class of low frequency oscillations, known as f and g-modes, have received particular atten-

tion because their  $l = 2$  multipolar component can couple with enough intensity to presently observed gravitational waves. Intensive work has been devoted to establish explicit relations between the frequency of different modes of pulsation and other properties of the star [43, 44, 45, 46, 47] or even with the EoS of the dense matter [45, 48, 49, 50, 51, 52, 53, 54, 55, 56].

The search for such kind of relations has been extended to other observables, with the aim of obtaining model independent interpretations of the observational data. The relations between the moment of inertia and the quadrupole moment in terms of the tidal Love number for slowly rotating stars are paradigmatic [57, 58, 35].

The description of the neutron stars based on microscopic models of the strong interaction still suffers from important uncertainties. The contrast between the recently obtained observational data and the predictions of a high variety of hadronic models [59, 60, 61, 62, 63, 64, 65, 66, 67, 68, 69, 70, 71, 72, 73, 74, 75, 76, 77, 78, 79] is a source for fix missing information. Many of these studies have assumed that matter is composed only by protons, neutrons and leptons. Hence the crucial requisite of neutron stars masses of at least  $M \simeq 2M_{\odot}$  is guaranteed [62]. A smaller number of investigations include effects of the hyperons [63, 64, 65, 66, 67, 68, 69, 72, 76, 79]. Furthermore, the possibility of a deconfinement phase transition taking place through different realizations has been studied [65, 66, 75]. First order transitions with discontinuous EoS have received special attention [60, 72, 73, 76] because their effects are more evident and would be detectable by the post-merger gravitational wave [72]. However the study of the observational data obtained so far is not conclusive. For instance, the analysis of the GW170817 event in [69] varies according to the amount of a priori information deposited on the sampling of EoSs. The probability for a free quark phase is 56% against 44% for a pure hadronic phase in one case, but an inverted 36% against 64% corresponds to the less informed sample. The analysis made in [75] including data from GW170817 and GW190425 events, does not find evidence of a strong phase transition.

The present work is mainly devoted to study the hyperon effects on the structure of neutron stars and on the pulsation modes propagating in their interiors. So it can be considered as the continuation of the previous study [79]. It is well known that neutron stars can support a stable hyperon population at densities well above the normal nuclear density, producing an energetically favorable state. At such densities the use of nuclear potentials which instantaneously propagates the strong interaction is not suitable. For this reason a covariant model of the field theory of hadrons is used in the mean field approach. The hyperons persist until extremely large densities, where the hadronic matter eventually undergoes a transition to a deconfined quark phase. The rise of the hyperon population as well as the deconfining transition significantly change the composition of the core of the star, producing a softer EoS. This, in turn, reduce the maximum mass achievable by the star. Thus, most of the models considering hyperons do not reach the measured value  $M/M_{\odot} \simeq 2$ . This situation is known in the literature as the hyperon puzzle [8].

In order to examine the ability of models containing hyperons to adjust recent astrophysical data, a composite description is proposed here. For extreme densities one can expect a deconfined quark phase which is treated within the Nambu-Jona Lasinio model (NJL) with vector interaction. For the hadronic phase, at medium densities, the hyperon-hyperon interaction is introduced together with polynomial meson-meson vertices. A continuous transition between such phases is assumed.

This work is organized as follows, in the next section the general theoretical description is presented. Section 3 is devoted to describe the evaluation of some properties of a neutron star. Specific results are shown and discussed in Sec. 4 and finally the conclusions are drawn in Sec. 5.

## 2 Theoretical description

For the hadronic phase a composition of models is considered. In the very low density regime, corresponding to the crust of the star, the scheme proposed in [80] will be used, as discussed below. It takes account of the nucleation of protons and neutrons in equilibrium, surrounded by a sea of electrons.

As the density is increased this nuclear system is replaced by a homogenous fluid of nucleons, according to the description of a model of the relativistic field theory of hadrons. Within this same framework, the onset of hyperons becomes energetically favorable for medium densities and they coexist with the nucleons. Finally, for sufficiently dense matter, the deconfined quarks emerge as the relevant degrees of freedom. In such case the Nambu- Jona Lasinio effective model of the strong interaction will be used.

In the intermediate density regime the strong interaction is represented by a model of baryons coupled linearly to mesons, and the latter exhibit polynomial vertices. The lagrangian density can be written as

$$\begin{aligned}
\mathcal{L}_H = & \sum_b \bar{\psi}_b (i \not{\partial} - M_b + g_{\sigma b} \sigma + g_{\xi b} \xi + g_{\delta b} \delta - g_{\omega b} \not{\omega} - g_{\phi b} \not{\phi} - g_{\rho b} \not{\rho}) \psi_b \\
& + \frac{1}{2} (\partial^\mu \sigma \partial_\mu \sigma - m_\sigma^2 \sigma^2) - \frac{A}{3} \sigma^3 - \frac{B}{4} \sigma^4 + \frac{1}{2} (\partial^\mu \delta \cdot \partial_\mu \delta - m_\delta^2 \delta^2) + G_{\sigma\delta} \sigma^2 \delta^2 \\
& + \frac{1}{2} (\partial^\mu \xi \partial_\mu \xi - m_\xi^2 \xi^2) + G_{\sigma\xi} \sigma^2 \xi^2 + G_{\xi\delta} \xi^2 \delta^2 - \frac{1}{4} W^{\mu\nu} W_{\mu\nu} + \frac{1}{2} m_\omega^2 \omega^2 \\
& - \frac{1}{4} R^{\mu\nu} \cdot R_{\mu\nu} + \frac{1}{2} m_\rho^2 \rho^2 + G_{\omega\rho} \rho^2 \omega^2 - \frac{1}{4} F^{\mu\nu} F_{\mu\nu} + \frac{1}{2} m_\phi^2 \phi^2 \quad (1)
\end{aligned}$$

where the sum runs over the octet of lightest baryons. In addition to the commonly used  $\sigma, \omega, \rho$  mesons, here the scalar iso-vector field  $\delta$ , as well as the hidden strangeness  $\xi, \phi$  mesons are also included. Here  $\delta$  and  $\rho$  stand for the third isospin component of these meson fields since the remaining components give null contribution in the approach used here [81].

The  $\delta$  and  $\xi$  particles can be identified with the  $a_0$  (980) and  $f_0$ (980) states, respectively. The  $\xi$  and  $\phi$  states are assumed as mainly composed by a  $s\bar{s}$  pair and therefore they couple only to the hyperons. Furthermore the values  $m_\phi = 1020$  MeV,  $m_\xi = 975$  MeV are adopted.

The Lagrangian (1) belongs to the framework of the Quantum Hadrodynamics [82]. The original model was progressively completed with additional meson-meson interactions with the aim to improve the agreement with the phenomenological knowledge. Thus, for instance, a better result for the compressibility was obtained by the inclusion of polynomial self-interaction in the scalar iso-scalar  $\sigma$  meson [83]. The density dependence of the symmetry energy was adjusted through vertices mixing the vector mesons  $\omega - \rho$  [84], as well as quartic  $\omega$  self-interaction was tuned to reproduce the maximum mass of a neutron star [85]. More recently a mixing term of the scalar  $\sigma - \delta$  mesons was proposed to improve the results for the radius of a neutron star and the tidal deformability of a binary system [86]. It must be noted that this development has focused on physical systems with increasing energy and matter densities as they become accessible to the experimental evidence. This work continues this line of

thought in the context of the hyperon puzzle. Two additional mixing vertices, not contemplated previously, are proposed here. They involve the scalar meson  $\xi$  which constitutes an exclusive channel for the hyperon interaction, and they reinforce the feedback with the nucleon fields.

The coupling constants  $g_{mb}$ ,  $m = \sigma, \xi, \delta, \omega, \rho, \phi$  and  $A, B, G_{\sigma\delta}, G_{\sigma\xi}, G_{\xi\delta}, G_{\omega\rho}$  are fixed to reproduce a set of selected empirical data. The  $\delta$  and  $\rho$  fields, in contrast with the other mesons, couple differently to each member of a baryon iso-multiplet since  $g_{\delta b}$ ,  $g_{\rho b}$  are proportional to the third projection of the isospin number of the baryon  $b$ .

The equations of motion corresponding to this Lagrangian are solved in the mean field approximation for uniform dense matter, in a reference frame where the mean value of the spatial component of the baryon currents are zero. Furthermore, all the degrees of freedom are considered as stable states of the strong interaction. Under such conditions the equations are greatly simplified, since the meson mean values do not vary spatially, and only the third component of the meson iso-multiplets are non-zero

$$(i \not{\partial} - M_b^* - g_{\omega b} \omega_0 - g_{\phi b} \phi_0 - g_{\rho b} \rho_0) \psi_b = 0,$$

$$(m_\sigma^2 - 2 G_{\sigma\delta} \delta^2 - 2 G_{\sigma\xi} \xi^2) \sigma + A\sigma^2 + B\sigma^3 = \sum_b g_{\sigma b} n_{sb},$$

$$(m_\delta^2 - 2 G_{\sigma\delta} \sigma^2 - 2 G_{\xi\delta} \xi^2) \delta = \sum_b g_{\delta b} n_{sb},$$

$$(m_\xi^2 - 2 G_{\sigma\xi} \sigma^2 - 2 G_{\xi\delta} \delta^2) \xi = \sum_b g_{\xi b} n_{sb},$$

$$(m_\omega^2 + 2 G_{\omega\rho} \rho_0^2) \omega_0 = \sum_b g_{\omega b} n_b$$

$$(m_\rho^2 + 2 G_{\omega\rho} \omega_0^2) \rho_0 = \sum_b g_{\rho b} n_b,$$

$$m_\phi^2 \phi_0 = \sum_b g_{\phi b} n_b$$

where  $M_b^* = M_b - g_{\sigma b} \sigma - g_{\xi b} \xi - g_{\delta b} \delta$  is the effective mass of the baryon  $b$ , and the source of the meson equations are the baryon densities

$$n_b = \frac{p_b^3}{3\pi^2}, \quad n_{sb} = \frac{M_b^*}{2\pi^2} \left[ p_b E_b - M_b^{*2} \ln \left( \frac{p_b + E_b}{M_b^*} \right) \right]$$

The left side equation introduces the Fermi momentum  $p_b$ , and  $E_b = \sqrt{p_b^2 + M_b^{*2}}$  is used. Within the approach, the energy density of the system is given by

$$\begin{aligned} \mathcal{E}_H &= \frac{1}{4} \sum_b (n_{sb} M_b^* + 3n_b E_b) + \frac{1}{2} (m_\sigma^2 \sigma^2 + m_\delta^2 \delta^2 + m_\xi^2 \xi^2 + m_\omega^2 \omega_0^2 + m_\rho^2 \rho_0^2 + m_\phi^2 \phi_0^2) \\ &\quad + \frac{A}{3} \sigma^3 + \frac{B}{4} \sigma^4 - G_{\sigma\delta} \sigma^2 \delta^2 - G_{\sigma\xi} \sigma^2 \xi^2 - G_{\xi\delta} \xi^2 \delta^2 + 3G_{\omega\rho} \omega_0^2 \rho_0^2 \end{aligned}$$

The pressure is obtained by the canonical relation at zero temperature

$$P = \sum_b \mu_b n_b - \mathcal{E}_H,$$

and the chemical potentials are given by  $\mu_b = E_b + g_{\omega b} \omega_0 + g_{\phi b} \phi_0 + g_{\rho b} \rho_0$ .

The bi-quadratic coupling between scalar mesons has been considered in [87] with the aim of studying how the properties of the neutron stars are affected by the mixing of the  $\sigma - \delta$  scalar mesons. The model was studied in [86], where the reference state for nuclear matter was fixed at the baryonic density  $n_0 = 0.16 \text{ fm}^{-3}$  and zero temperature. At such point the following empirical values  $E_{\text{bind}} = -16 \text{ MeV}$ ,  $E_{\text{sym}} = 32 \text{ MeV}$ ,  $M_N^*/M_N = 0.65$ ,  $K = 230 \text{ MeV}$ , and  $L = 50 \text{ MeV}$  were adopted for the binding energy, the symmetry energy, the effective nucleon mass ( $N = n, p$ ), the nuclear compressibility and the slope parameter of the symmetry energy respectively. They serve as constraints to determine the constants  $g_{\sigma N}, g_{\omega N}, A$  and  $B$ , and to give a reasonable range of variation for  $g_{\delta p}, g_{\rho p}, G_{\omega\rho}$  and  $G_{\sigma\delta}$ . An examination of the predictions for the tidal deformability  $\Lambda_{1.4}$  has shown that larger values of  $G_{\sigma\delta}$  improves the agreement with the constraints provided by the GW170817 event [86]. A further extension was presented in [79] introducing hyperons as well as the  $\phi$  vector meson. The couplings between hyperons and vector mesons were fixed according to the SU(6) symmetry of the quark model

$$\begin{aligned} g_{\omega\Lambda} = g_{\omega\Sigma} = 2g_{\omega\Xi} &= \frac{2}{3}g_{\omega N}, \\ g_{\rho\Lambda} = 0, \frac{1}{2}g_{\rho\Sigma^+} = g_{\rho\Xi^0} &= -\frac{1}{2}g_{\rho\Sigma^-} = -g_{\rho\Xi^-} = -g_{\rho n} = g_{\rho p}, \\ g_{\phi\Lambda} = g_{\phi\Sigma} = \frac{1}{2}g_{\phi\Xi} &= -\frac{\sqrt{2}}{3}g_{\omega N}. \end{aligned}$$

The three parameters  $g_{\sigma b}$ ,  $b = \Lambda, \Sigma, \Xi$  are determined by adjusting the energy  $U_b = g_{\omega b} \omega - g_{\sigma b} \sigma$  of an isolated hyperon at rest, immersed in isospin symmetric nuclear matter at the normal density. Although their empirical values are poorly known, they are usually taken as

$$U_\Lambda = -30 \text{ MeV}, U_\Sigma = 30 \text{ MeV}, U_\Xi = -18 \text{ MeV}. \quad (2)$$

The values  $g_{\sigma\Lambda} = 5.616$ ,  $g_{\sigma\Sigma} = 3.989$ , and  $g_{\sigma\Xi} = 2.920$  are thus obtained. In contrast to the simplifications made in [79], the coupling between the hyperons and the scalar mesons  $\xi$  and  $\delta$  are fully considered here. The latter distinguishes the components of a baryonic isospin multiplet, and particularly does not couple to those hyperons with zero third isospin component  $I_b = 0$ , hence  $g_{\delta\Lambda} = g_{\delta\Sigma^0} = 0$ . In addition the assumption that the strength of its coupling to a given baryon decreases with its strangeness content leads one to  $2g_{\delta p}/3 = g_{\delta\Sigma^+} = g_{\delta\Xi^0}$ , opposite signs must be assigned to the complementary isospin projections  $g_{\delta n} = -g_{\delta p}$ ,  $g_{\delta\Sigma^-} = g_{\delta\Xi^-} = -2g_{\delta p}$ . The vertices involving the  $\xi$  meson are exclusive for the hyperons, hence they could be deduced from the scarce information on hyperon matter [88, 89]. As a phenomenological guide one can consider the criterium that relates the excess binding energy  $\Delta B(A)$  of a double  $\Lambda$  hypernucleus of atomic number  $A$  to the single particle potential  $U_\Lambda^{(\Lambda)}(n)$  in  $\Lambda$  matter at density  $n$ , i. e.

$$\Delta B(A) \simeq U_\Lambda^{(\Lambda)}(n) - 2U_\Lambda^{(\Lambda)}(2n) \simeq -U_\Lambda^{(\Lambda)}(n)$$

where  $n \simeq n_0/A$  [89], and  $\Delta B(6) = 0.67 \text{ MeV}$  is identified as the experimental value of the  ${}^6_{\Lambda\Lambda}He$  hypernucleus, see for instance [90]. Thus the constraint  $U_\Lambda^{(\Lambda)}(n_0/5) = -0.67 \text{ MeV}$  is adopted here in agreement with other investigations on compact stars [91, 92, 93].

Following the arguments of [88], the single particle potentials of the  $\Xi$  and  $\Lambda$  hyperons are related by

$$U_{\Xi}^{(\Xi)}(n_0) = 2 U_{\Lambda}^{(\Lambda)}(n_0/2)$$

The strategy to fix the remaining constants of the model is to explore the bidimensional space  $G_{\sigma\xi}$   $G_{\xi\delta}$  with the aim of accommodating neutron stars with mass  $M \simeq 2M_{\odot}$ . In the process it was found that the value of  $G_{\xi\delta}$  is irrelevant due to the smallness of the product  $\xi^2 \delta^2$ , therefore  $G_{\xi\delta} = 0$  is taken from here on. The numerical values of the remaining parameters are as follows:  $m_{\sigma} = 500$  MeV,  $m_{\delta} = 983$  MeV,  $m_{\omega} = 783$  MeV,  $m_{\rho} = 770$  MeV,  $A=13.08$  fm $^{-1}$ ,  $B=-31.6$ ,  $g_{\sigma N} = 9.22$ ,  $g_{\omega N} = 11.35$ ,  $g_{\delta p} = \sqrt{5.2\pi}$ ,  $g_{\rho p} = \sqrt{11.08\pi}$ ,  $G_{\sigma\delta} = 50$ ,  $G_{\sigma\xi} = -100$ ,  $G_{\omega\rho} = 263.92$ ,  $g_{\xi\Lambda} = 2.117$ , and  $g_{\xi\Xi} = 10.077$ . The criterium to select this specific value for  $G_{\sigma\xi}$  is discussed in Sec.4.

The hypothesis of homogeneous matter which leads to the equations of motion shown above, is appropriate for densities greater than several tenths of the normal nuclear value  $n_0$ . The electromagnetic interaction, not included in (1), gives rise to non-homogeneous structures. For this reason the EoS evaluated in [80] is adopted for the low density regime and assembled to the results of the interaction (1) by imposing continuity at the matching point  $n = 0.35n_0$ .

For very dense matter it is expected that hadrons are not longer the most stable configuration and a transition to deconfined quarks happens. To take account of this state of homogeneous quark matter, the NJL model is implemented with inclusion of a vector interaction [94]. The NJL presents interacting quarks which generate their own constituent masses. This effective mass depends on the properties of the medium and are expected to decrease with increasing baryonic density.

The energy density is given by

$$\mathcal{E}_Q = \sum_q \left[ \frac{N_c}{\pi^2} \int_{\Lambda}^{p_q} dp p^2 \sqrt{p^2 + M_q^2} + 2G n_{sq} + 18G_v n_q^2 \right] - 4K n_{su} n_{sd} n_{ss} + \mathcal{E}_0 \quad (3)$$

where  $q = u, d, s$ ,  $p_q$  is the Fermi momentum which is related to the baryonic number density by  $n_q = p_q^3/3\pi^2$ .

The effective masses are given by

$$M_i = m_i - 4G n_{si} + 2K n_{sj} n_{sk}, \quad j \neq i \neq k.$$

where  $m_q$  is the current quark mass, and the quark condensates  $n_{sq}$  can be expressed as

$$n_{sq} = \frac{N_c}{\pi^2} M_q \int_{\Lambda}^{p_q} \frac{dp p^2}{\sqrt{p^2 + M_q^2}}$$

A cutoff  $\Lambda$  is used to renormalize ultraviolet divergences in the momentum integration,  $\mathcal{E}_0$  is a constant introduced to obtain zero vacuum energy,  $G$  and  $K$  are the couplings for four and six quark interactions, and  $G_v$  is the strength of the vector current-current interaction. The chemical potential for each flavor is simply  $\mu_q = \sqrt{p_q^2 + M_q^2} + 12G_v n_q$ .

For the numerical calculations the set of constants specified in [95] are used. The vector coupling  $G_v$  has not been determined with precision and it is usually taken as a parameter within the range  $0 \leq G_v \leq G$ . Therefore the relatively low value  $G_v = 0.08G$  is chosen here in order to obtain a threshold density  $n \geq 4n_0$  for the deconfinement process.

The transition between the hadronic and deconfined phases has been described within different dynamical schemes. In this work the picture of a continuous and monotonous EoS, with an intermediate state of coexisting phases is adopted. It is commonly denominated as the Gibbs construction. If  $\chi$  is the spatial fraction occupied by the deconfined phase, then the total energy and the baryonic number densities of the system are given by

$$\mathcal{E} = \chi \mathcal{E}_Q + (1 - \chi) \mathcal{E}_H, \quad (4)$$

$$n = \chi n_Q + (1 - \chi) n_H \quad (5)$$

Furthermore, for thermodynamical equilibrium of the coexisting phases the partial pressures of each phase must coincide

$$P_B = \sum_b \mu_b n_b - \mathcal{E}_H = \sum_q \mu_q n_q - \mathcal{E}_Q. \quad (6)$$

To describe neutron star matter the complementary requirement of electrical neutrality is imposed. To reach this condition a fluid of non-interacting leptons (electrons and muons) is considered, which freely distributes among the hadron and quark phases so that the condition

$$0 = 3\chi \sum_q C_q n_q + (1 - \chi) \sum_b C_b n_b - \sum_l n_l, \quad (7)$$

is satisfied. In this expression  $C_k$  stands for the electric charge in units of the positron charge.

These leptons also contribute to the total energy by

$$\mathcal{E}_L = \frac{1}{\pi^2} \sum_l \int_0^{p_l} dp p^2 \sqrt{p^2 + m_l^2}$$

where  $n_l = p_l^3/3\pi^2$ , their chemical potentials can be written as  $\mu_l = \sqrt{p_l^2 + m_l^2}$ , and the partial lepton contribution to the pressure is  $P_L = \sum_l \mu_l n_l - \mathcal{E}_L$ . Hence, the complete expressions for the energy and the pressure in the mixed phase are

$$\mathcal{E} = \chi \mathcal{E}_Q + (1 - \chi) \mathcal{E}_H + \mathcal{E}_L, \quad (8)$$

$$P = \mu_B n - \mathcal{E} = P_B + P_L. \quad (9)$$

The coefficient  $\chi$  is obtained by using the conditions of conservation of the baryonic number, the electric charge, and thermodynamical equilibrium, Eqs. (5), (7) and (6) respectively. Thus, it is uniquely determined for each density of neutral matter in equilibrium at zero temperature, and it is a dynamical property of the combination of models used.

There are two conserved charges which characterize the global state of the system, the baryonic number and the electric charge with associated chemical potentials  $\mu_B$  and  $\mu_C$  respectively. It must be noted that the last one does not enter in the intermediate expression of Eq. (9) because the total electric charge is zero. Both chemical potentials can be combined to give the chemical potentials of all baryons, quarks and leptons circumstantially present. Therefore they are linearly dependent through the relations of equilibrium against beta decay.



### 3 Properties of the neutron star

The structure of an isolated neutron star can be solved using the Tolman-Oppenheimer-Volkov equations for the spherically symmetric case

$$\begin{aligned}\frac{dP}{dr} &= -[\mathcal{E}(r) + P(r)][\mathcal{M}(r) + 4\pi r^3 P(r)] \frac{e^{2\lambda(r)}}{r^2}, \\ \mathcal{M}(r) &= \int_0^r 4\pi r'^2 \mathcal{E}(r') dr' .\end{aligned}$$

Units for which  $c = 1$ ,  $G = 1$ ,  $\hbar = 1$  has been used. The relation  $\mathcal{E}(P)$  is provided by the EoS described in the previous section and the definition

$$e^{\lambda(r)} = [1 - 2\mathcal{M}(r)/r]^{-1/2}$$

is used.

Starting from given values of the central pressure and energy, these equations are integrated outward until a radius  $R$  is reached for which  $P(R) = 0$ , and the total mass is defined as  $M = \mathcal{M}(R)$ .

Once the mass  $\mathcal{M}(r)$  and pressure  $P(r)$  distributions inside the star have been determined one can evaluate its moment of inertia  $I$  assuming slow and homogeneous rotation with angular velocity  $\Omega$ . By solving the differential equation for  $\varphi(r) = 1 - \omega(r)/\Omega$ , where  $\omega(r)$  is the angular velocity distribution of a fluid element inside the star [96]

$$\frac{d}{dr} [r^4 j(r) \varphi'(r)] + 4r^3 j'(r) \varphi(r) = 0, \quad r < R \quad (10)$$

with the definition  $j(r) = \exp -[\lambda(r) + \nu(r)]$ , and the metric function  $\nu(r)$  satisfies the equation

$$\frac{d\nu}{dr} = -\frac{dP/dr}{\mathcal{E}(r) + P(r)}$$

and the auxiliary condition  $e^{\nu(R)} = e^{-\lambda(R)}$ .

The solution outside the star is

$$\varphi(r) = 1 - \frac{2I}{r^3}, \quad r > R.$$

Thus, Eq. (10) is complemented with the boundary conditions  $\varphi'(0) = 0$ ,  $\varphi(R) = 1 - 2I/R^3$ .

The tidal deformability of a compact star can be written in terms of the second Love number  $k_2$  as  $\Lambda = 2k_2/3x^5$ , where the compactness parameter is  $x = M/R$ . To evaluate the Love number the radial function  $y(r)$ , related to the tidal field, must be found by solving the differential equation

$$y'(r) + y^2(r) + f(r)y(r) + q(r)r^2 = 0$$

subject to the condition  $y(0) = 2$ . The following definitions has been used

$$\begin{aligned}f(r) &= [1 + 4\pi r^2 (P - \mathcal{E})] e^{2\lambda(r)} \\ q(r) &= \left[ 4\pi \left( 5\mathcal{E} + 9P + \frac{P + \mathcal{E}}{v_e^2} \right) - \frac{6}{r^2} - \frac{4}{r^4} \frac{(\mathcal{M} + 4\pi r^3 P)^2}{1 - 2\mathcal{M}/r} \right] e^{2\lambda(r)}\end{aligned}$$

The relativistic speed of sound  $v_e$  has been introduced, which is defined by

$$v_e^2 = c^2 \frac{dP}{d\mathcal{E}}. \quad (11)$$

Finally, the Love number is given by

$$\begin{aligned}
k_2 &= \frac{8}{5}x^5(1-2x)^2[2-y_R+2x(y_r-1)]/\left\{6x[2-y_R+x(5y_R-8)]\right. \\
&+ 4x^3[13-11y_R+x(3y_R-2)] \\
&+ \left.2x^2(1+y_R)\right\}+3(1-2x)^2[2-y_R+2x(y_R-1)]\ln(1-2x)\}
\end{aligned}$$

where  $y_R = y(R)$ .

In order to simplify the numerical evaluation of the oscillatory motion inside the star an approximation, known as the relativistic Cowling approach will be used. It consists in neglecting the variation of the metric functions of the space-time supporting the vibrations [41]. The discrepancy between full calculations and those using the Cowling treatment was studied long time ago [97], and repeated under various conditions [98, 99]. These investigations found that the difference is of the order 10 – 30 %. This work intends a qualitative description for stars with masses greater than  $2M_\odot$ , therefore this approach is adequate and a discrepancy of about 20% in the oscillation frequencies is expected.

Assuming spherical symmetry for the equilibrium state, the displacement of a fluid element located at point  $r, \theta, \phi$  at time  $t$  can be decomposed in a multipolar expansion as

$$\delta r = \frac{e^{-\lambda}}{r^2} W(r) Y_l^m(\theta, \phi) e^{i\omega t}, \quad (12)$$

$$\delta \theta = -\frac{V(r)}{r^2} \frac{\partial}{\partial \theta} Y_l^m(\theta, \phi) e^{i\omega t}, \quad (13)$$

$$\delta \phi = -\frac{V(r)}{r^2 \sin^2 \theta} \frac{\partial}{\partial \phi} Y_l^m(\theta, \phi) e^{i\omega t}. \quad (14)$$

In this approach the unknown functions  $W(r), V(r)$  satisfy the differential equations

$$\begin{aligned}
\frac{dV}{dr} - 2\frac{d\nu}{dr}V + \frac{e^\lambda}{r^2}W - \left(\frac{1}{v_e^2} - \frac{1}{v_a^2}\right)\left(V + e^{2\nu-\lambda}\frac{d\nu}{dr}\frac{W}{(r\omega)^2}\right)\frac{d\nu}{dr} &= 0, \\
\frac{dW}{dr} + l(l+1)e^\lambda V - \frac{1}{v_a^2}\left(r^2\omega^2 e^{\lambda-2\nu}V + \frac{d\nu}{dr}W\right) &= 0
\end{aligned}$$

and they are subject to the conditions

$$\begin{aligned}
W(r) + l r V(r) &\rightarrow 0, \text{ as } r \rightarrow 0, \\
R^2\omega^2 V(R) + \nu'(R) e^{3\nu(R)}W(R) &= 0.
\end{aligned}$$

The equations above contain the adiabatic speed of sound, defined by

$$v_a^2 = c^2 \frac{\partial P}{\partial \mathcal{E}}, \quad (15)$$

where the partial derivative is evaluated by keeping constant the relative population of each fermionic species, and the constraint of  $\beta$  equilibrium is imposed after evaluation. The velocity is related to the adiabatic index by the relation  $\gamma P = (P + \mathcal{E}) v_a^2$ . The differences between  $v_e$  and  $v_a$  has been previously discussed, as for instance in [52].

In our approach the relation between  $P$  and  $\mathcal{E}$  is monotonous and continuous,

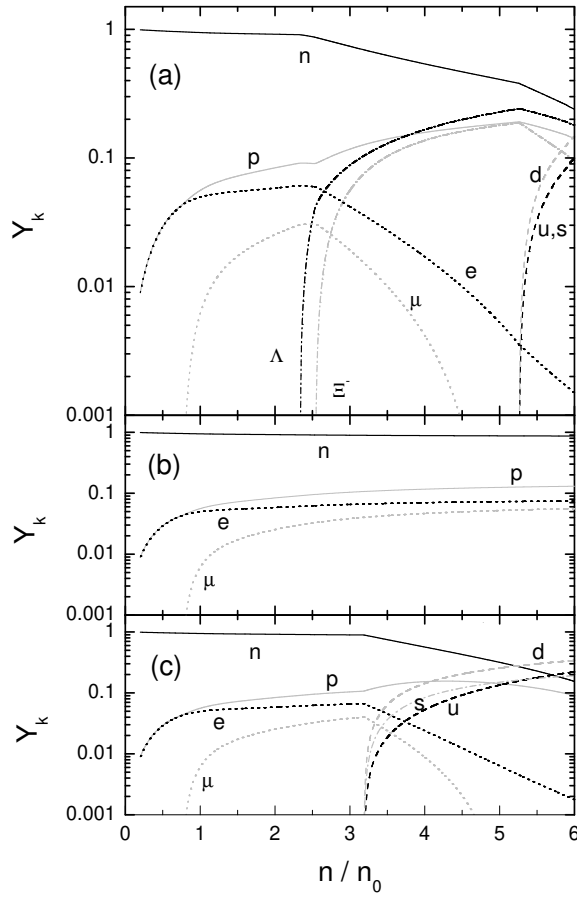


Figure 1: The partial fraction  $Y_k$  for the different species considered in the approaches F (a), N (b), and NQ (c). The definitions  $Y_b = (1 - \chi) n_b/n$  for baryons,  $Y_q = \chi N_c n_q/n$  for quarks, and  $Y_l = n_l/n$  for leptons, are used. The abbreviation F stand for the case with the full octet of baryons and quarks, N for the case with only nucleons, and NQ for the case of nucleons combined with quarks, in agreement with the convention stated in the main text.

however its first derivative, i. e. the speed of sound  $v_e$ , presents finite discontinuities at the threshold of the phase transition.

Explicit expressions for  $v_e$  and  $v_a$  can be found in [79].

The quantity

$$A_+ = -\frac{d\nu}{dr} (v_e^{-2} - v_a^{-2}) e^{-\lambda}$$

discriminates convective instability by the condition  $A_+ > 0$ . Furthermore, it is related to the Brunt-Väisälä frequency  $N$  by

$$N^2 = -e^\nu A_+ d\nu/dr. \quad (16)$$

## 4 Results and discussion

In this section an analysis of the EoS of the model proposed and its ability to adjust the relevant information provided by the observational evidence about compact stars is made. It must be mentioned that the model tries to cover a wide range of phenomenological results but keeping simple. The classical description given in [80] takes account of the emergence of atomic nuclei at low

densities. The covariant field theory of hadrons is appropriate for medium densities where relativistic effects becomes important and the homogeneity of matter is a plausible assumption. Furthermore new hadronic and leptonic degrees of freedom, relevant for the composition of a neutron star, are easily included. Finally for the highest densities achievable in the core of a compact star, it is expected that hadrons are replaced by deconfined quarks. The NJL framework is adopted for this stage, since it effectively represents the strong interaction for the energy regime involved.

The determination of the parameters of the model follows this staggered scheme, the masses and couplings of the conventional degrees of nuclear physics are fixed using the well established phenomenology at the normal density  $n_0$ . More uncertain are the parameters of the hyperonic interaction due to the lack of precise experimental data. For instance, the hyperon-nucleon interaction mediated by the scalar  $\sigma$  meson is normalized by the single hyperon potentials in nuclear matter. The coupling of the hidden strangeness  $\xi$  meson, responsible of the hyperon-hyperon interaction, is deduced using single hyperon potentials in hyperonic matter. Other constants are chosen to improve the agreement with astrophysical data. This is the case of the constant  $G_{\sigma\delta}$ , whose preferable value for adjusting the tidal deformability  $\Lambda_{1.4}$  was discussed in [86]. A similar case is found for the vector current-current coupling of the NJL. Since an increase of  $G_v$  has the effect of enlarging the deconfinement density as well as the central density while decreasing the radius of the maximum mass star, the value  $G_v = 0.08 G$  was chosen in order to optimize the coincidence with the result  $M_{\max} \simeq 2 M_\odot$ .

In regard of the coupling  $G_{\sigma\xi}$  one can expect numerical values comparable to  $G_{\sigma\delta}$  obtained in [86], with the necessary modification to take account of the expected smaller amplitude of  $\xi$  as compared to  $\delta$ . Thus the range  $|G_{\sigma\xi}| \leq 100$  has been initially explored. By changing its numerical value, but keeping the constraint on the single particle potentials of the hyperons, an increasing trend on the maximum mass of a neutron star was obtained as  $G_{\sigma\xi}$  is decreased. Thus for  $G_{\sigma\xi} = 0, -20, -60$  the results  $M_{\max}/M_\odot = 1.94, 1.96, 1.98$  are obtained for a particular value of  $G_v$ .

As a first probe the partial fraction of baryons and leptons is examined in Fig. 1. The results for the full treatment (F) are displayed in the upper panel, while the bottom one combines the case with nucleons and leptons only (N), together with that considering nucleons, leptons, and quarks (NQ). As it is usual, the onset of the hyperons  $\Lambda$  and  $\Xi^-$  at densities near  $2.3 n_0$  causes a pronounced decrease of the population of leptons, and particularly of the muons that are extinguished around  $n/n_0 = 4.5$ . The fraction of neutrons is also diminished in contrast with the slight rise shown by the protons. At a higher density  $n/n_0 = 5.3$  starts the coexistence with a phase of deconfined quarks, which produce the final decline of all the baryonic species. It must be mentioned that within this approach the core of the more massive neutron star has a considerable fraction of hadrons, i.e. no pure quark matter is found there.

The case N shows that if hyperons and quarks were suppressed, the composition of beta equilibrated matter becomes asymptotically stable with increasing density (Fig.1b). However if a continuous transition from nuclear to quark matter is allowed, as in the NQ case Fig.1c, the deconfinement happens at a lower density  $n/n_0 \simeq 3.2$ .

The EoS obtained in this model is shown in Fig.2. A low energy regime, consisting of pure nuclear matter and leptons, is distinguished by the coincidence of the three cases F, N, and NQ. The  $\Lambda$  hyperon becomes stable at a

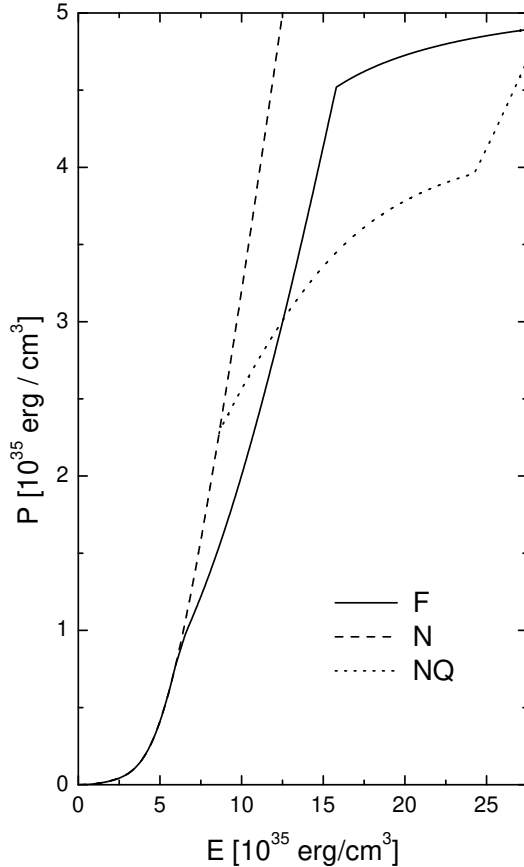


Figure 2: The equation of state for the composite model, the different approaches are distinguished according to the line convention shown. As expected the EoS becomes softer around the hyperon onset and the deconfinement threshold. Hence the case N exhibits the steepest EoS, while the curve F keeps harder than the NQ one because of its delayed deconfinement transition. The abbreviations F, N, and NQ are described in the caption of Fig. 1.

density  $n = 2.3 n_0$ , corresponding to the split of the F and N curves. The  $\Xi^-$  also appears before the coexistence with deconfined quarks takes place. This fact is marked by a sudden change in the tangential direction of the curve F. On the other hand, pure nuclear matter becomes unstable earlier, at the point where the N and NQ curves separate. While the upper part of the NQ curve shows the end of the coexistence regime. As expected, the inclusion of configurations that minimize the energy of the system leads to a softening of the EoS. The pressure at the density  $n/n_0 = 2$  has been estimated in [39] as  $P = 3.5_{-1.7}^{+2.7} \times 10^{34}$  dyn/cm<sup>2</sup> in order to be consistent with the observational data of the GW170817 event. In the present calculations the result  $P = 4.2 \times 10^{34}$  dyn/cm<sup>2</sup> has been obtained, which is comprised within the confidence band.

An interesting fact can be appreciated in Fig. 3, which shows the neutron and proton masses as functions of the density. The presence of the hyperons makes the decrease of the nucleon masses more pronounced. In particular the neutron mass is almost collapsed when the deconfinement starts. In the mixed phase, instead, it increases slightly so that the mass difference of the duplet is considerably reduced. The same feature is repeated in the case of only nucleons coexisting with unbound quarks.

The behavior of the masses is a consequence of the variance of the amplitude of the scalar fields, as shown in Fig. 4. The increase of the  $\sigma$  meson has an additional source in the  $\sigma^2 \xi^2$  vertex which becomes active at the onset of the  $\Lambda$

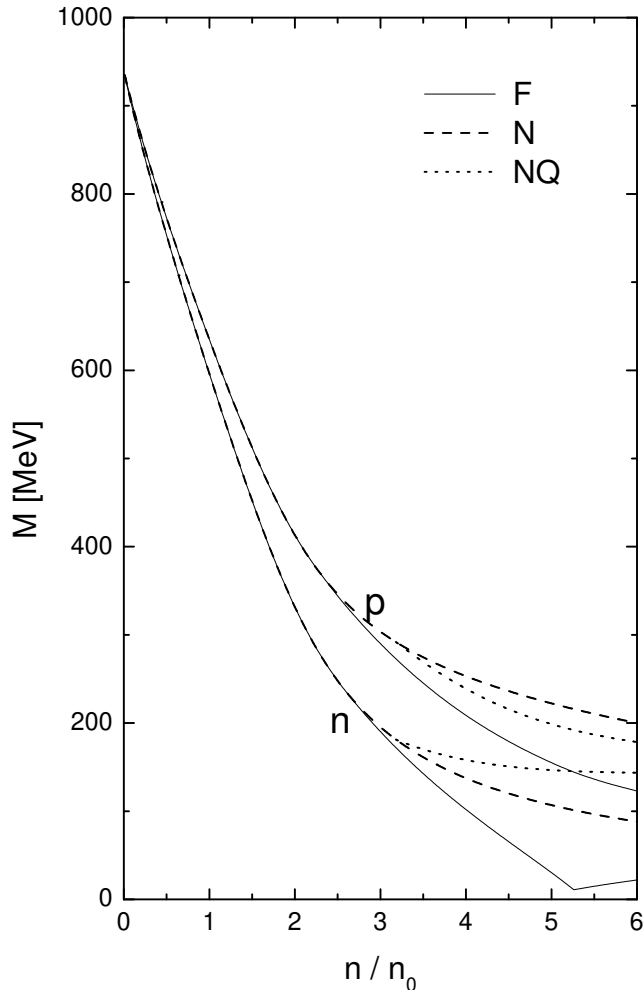


Figure 3: The mass of the proton-neutron duplet as functions of the baryonic density for different approaches. For each of these nucleons the three curves coincide below the hyperon onset. Above the deconfinement threshold the case F shows the lightest masses. While for the N and NQ instances, the results are opposite for protons and neutrons. This is a consequence of the weakness of the  $\delta$  meson in the coexistence phase, favoring the degeneracy of the masses of the nucleons. The abbreviations F, N, and NQ are described in the caption of Fig. 1.

hyperon (F case). However the  $\xi$  mean field decreases in the mixed phase as the hyperon population diminishes. This effect is reinforced by the simultaneous decrease of the amplitude of the  $\delta$  meson.

In a certain sense the exclusive hyperon-hyperon interaction gives physical continuity to the model. The exchange of the  $\phi$  and  $\xi$  mesons represent the vector and scalar channels contributing to the repulsive and attractive terms of the EoS, respectively.

These contributions are balanced by reproducing the empirical data proposed for multi-hyperon systems [88, 89, 90]. The former promotes the deconfinement transition by matching opportunely the EoS provided by the NJL. The latter favors the high density regime of the nucleon masses shown in Fig. 3, mimicking the dynamical recovery of chiral symmetry. Although this is not the real case because the coupling between nucleons and the scalar mesons are still active. Hence if one tries  $G_{\sigma\xi} = 0$ ,  $g_{\phi Y} = 0$ ,  $g_{\xi Y} = 0$  then the deconfinement transition will not be reached, and the trends of the hadronic results will continue until the collapse of the neutron mass determines the limit of applica-

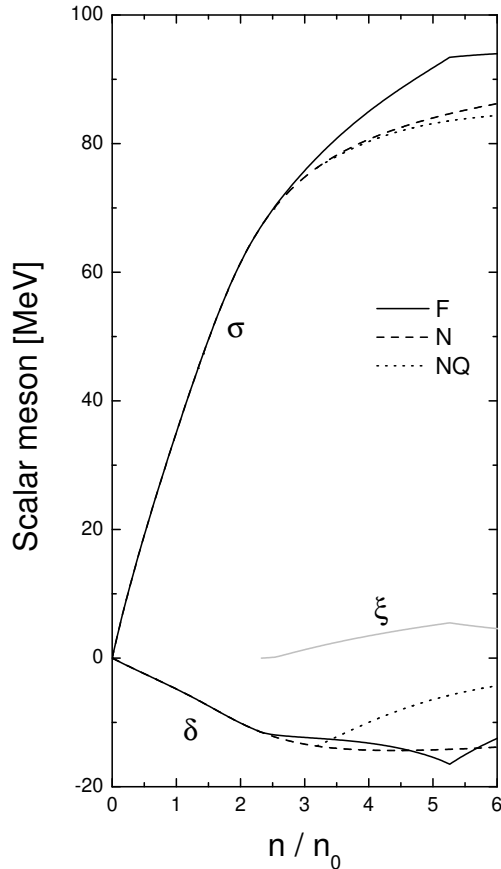


Figure 4: The amplitude of the mean field solutions for the scalar mesons  $\sigma$ ,  $\delta$ , and  $\xi$  as functions of the baryonic density for different approaches. It is remarkable the strengthening of the  $\sigma$  meson (case F) beyond the hyperon onset due to the feedback with the  $\xi$ . While the coexistence of phases causes a decrease of the amplitude of all the mesons (cases F and NQ).

bility of the model. One can conclude that in the present work the two models approach is necessary and they are really complementary. As discussed in the previous paragraphs, the parameters of the model can not be completely determined by the experimental constraints and there is some extent of freedom in their choice. Some judicious assumptions have been made in the present work, and the effect of their variance deserves further investigation.

The EoS just described are used as input to solve the macroscopic properties of a non rotating neutron star, as for instance the mass-radius relation shown in Fig. 5. The maximum masses are  $M/M_{\odot} = 2.01, 2.45,$  and  $2.17$ , whereas the corresponding radius are  $R = 11.7, 11.7,$  and  $12.5$  in the F, N, and NQ treatments, respectively. The central density of such stars are  $n/n_0 = 6.35, 5.33,$  and  $4.95$ , so that the core of the star does not support pure quark matter. However, in the F and NQ cases it is composed of an admixture of hadrons and deconfined quarks.

The radius of a neutron star could bring important information on the underlying EoS [101], therefore it is interesting to make a comparison with the Bayesian analysis presented in [22] for the massive pulsar PSR J0740+6620. It obtains the radius  $R = 12.39^{+1.30}_{-0.98}$  for the star with  $M/M_{\odot} = 2.072^{+0.067}_{-0.066}$ . The main result of this work, i.e. F case, is compatible with these constraints and therefore the presence of hyperons as well a deconfinement transition are not ruled out by them.

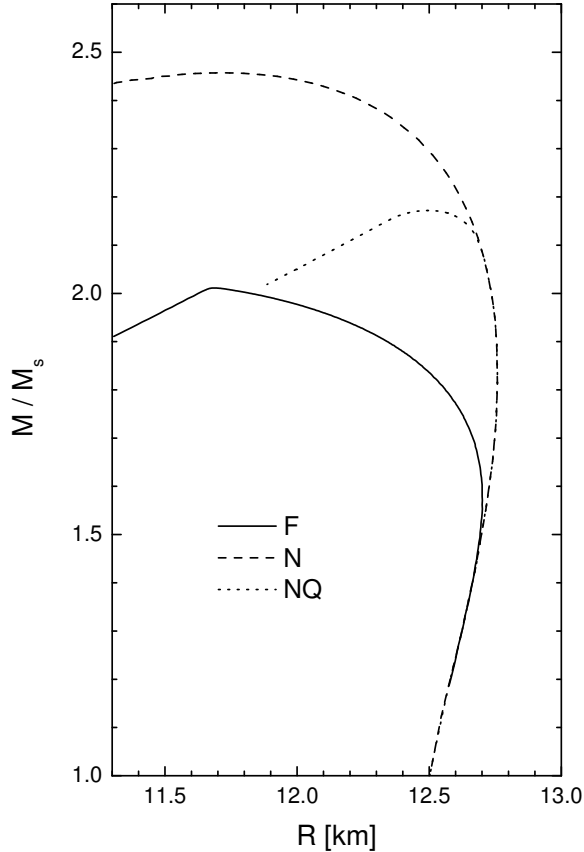


Figure 5: The mass-radius relation for neutron stars for different approaches. As expected, the greatest mass corresponds to the case where only conventional degrees of freedom are used (N). When a transition to deconfined quarks is allowed,  $M_{\max}$  decreases but the corresponding radius is relatively large (NQ). In the full treatment  $M_{\max}$  is slightly greater than two solar masses (F). The abbreviations F, N, and NQ are described in the caption of Fig. 1.

In regard of the neutron star with the standard  $M/M_{\odot} \simeq 1.4$  mass, in the present work it is found mainly composed by nucleons and a tiny 1% of  $\Lambda$  hyperons in the core of the star. The corresponding radius  $R_{1.4} = 12.66$  km can be contrasted with the estimates  $12.33^{+0.76}_{-0.81}$  km and  $12.18^{+0.56}_{-0.79}$  km obtained by different approaches in [24], or the result  $R_{1.4} = 12.45 \pm 0.65$  km obtained in [102].

At this point a general comparison with previous works using similar conceptual tools as in the present investigation is opportune. All of them use a hadronic field model with hyperons and combined with NJL in a continuous phase transition. The partial contribution of baryons and quarks to the composition of stellar matter is in qualitative coincidence with the calculations shown in [100]. This reference considers two versions of the NL3 (TM1) parametrization, obtaining a deconfinement threshold located around  $n_t/n_0 = 3.1$  (4.4), the maximum mass is approximately  $2.03 M_{\odot}$  ( $1.65 M_{\odot}$ ) and the corresponding radius  $R \simeq 13.6$  km ( $R \simeq 13.3$  km). In all the cases the fiducial star with  $M/M_{\odot} = 1.4$  has a large radius  $R_{1.4} > 14.2$  km. The same quantities as evaluated in [66] are  $n_t/n_0 = 2.3$ ,  $M_{\max}/M_{\odot} \simeq 2.2$  and  $R \simeq 13.2$  km, however the authors discard this approach due to the impossibility to adjust reasonable values for the tidal deformability. In addition the outcomes of [108] place the transition at  $n_t/n_0 = 2.7$ , besides  $M_{\max}/M_{\odot} \simeq 2.55$ ,  $R \simeq 14.2$  km and  $R_{1.4} = 14.5$  km.



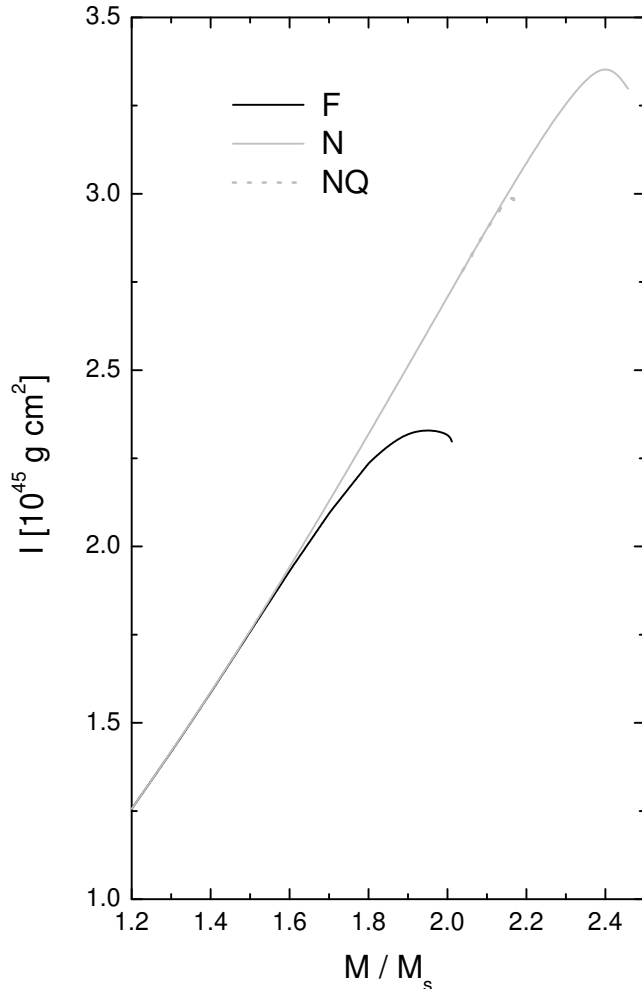


Figure 6: The moment of inertia of a slowly rotating neutron star in terms of the star mass for different approaches. This quantity is defined as  $I = R^3 [1 - \varphi(R)] / 2$ , where  $\varphi$  is the solution of the differential equation (10). The curve NQ is almost indistinguishable from the curve N, but it finishes below  $n/n_0 \simeq 2.2$ .

As a partial conclusion it can be stated that the present treatment produces the highest threshold density for the deconfinement transition, noticeably improves the result for  $R_{1.4}$  and gives a reasonable maximum mass.

The effect of the mixing vertex for the  $\sigma - \xi$  mesons is clarified by contrasting with the outcomes of the related model used in [79]. The deconfinement threshold density is shifted towards higher values, a significant increase of almost 26% is obtained in the F case. The properties of the maximum mass star, instead, are slightly modified. The value for  $M_{max}$  is raised by less than 1%, whereas the corresponding radius is decreased by a 6%. The main features of the fiducial star remain practically unchanged because of the tiny fraction of hyperons present in such case.

The moment of inertia of a slowly rotating star is presented in Fig. 6 as a function of the inertial mass. The presence of hyperons is discernible only for stars with  $M \simeq 2 M_\odot$  due to the fact that the moment of inertia takes a maximum value before  $M_{max}$  is reached. The candidate for an imminent precision measurement PSR J0737-3039A has a mass  $M/M_\odot = 1.338$ , for which the analysis made in [16] suggest  $I = 1.36^{+0.15}_{-0.32} \times 10^{45} \text{ g cm}^2$ . In the present

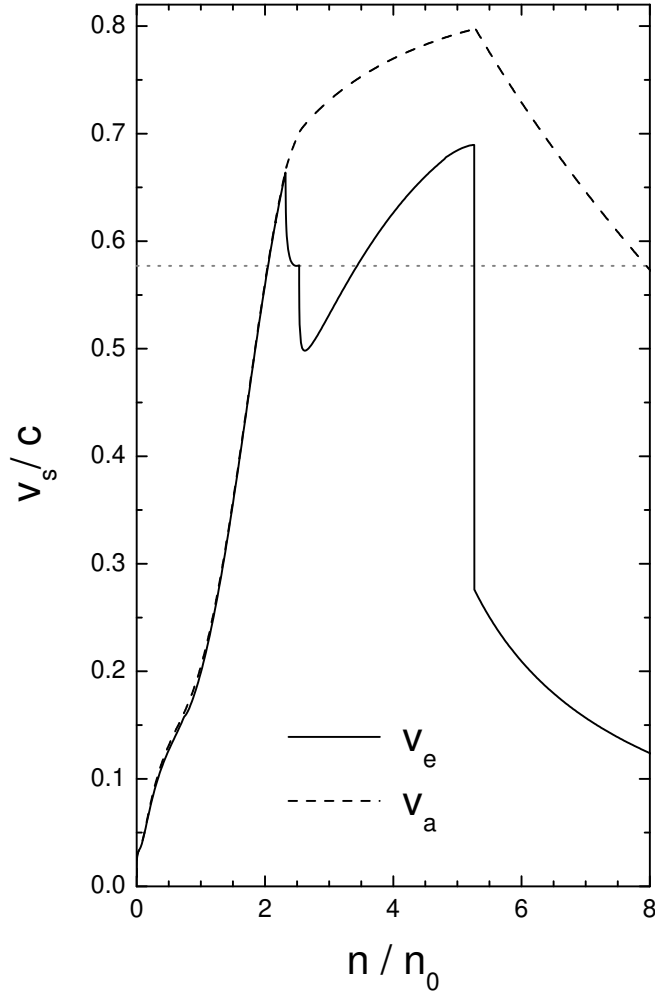


Figure 7: The equilibrium  $v_e$  and adiabatic  $v_a$  speeds of sound as functions of the baryonic density in the F case. The horizontal line corresponds to the conformal limit. The definitions of both speeds are given in Eqs. (11) and (15).

calculations the result is  $I = 1.48 \times 10^{45} \text{ g cm}^2$ , which is slightly greater than the most probable value given there, but within the confidence band. The same conclusion holds respect to the prediction  $I = 1.15^{+0.38}_{-0.24} \times 10^{45} \text{ g cm}^2$  given in [35]. It must be mentioned that within the model used here, such star would have a central density  $n \simeq 2.3n_0$  and therefore would be composed only by nucleons and leptons.

Calculations of the adimensional moment  $\tilde{I} = I/MR^2$  in terms of the compactness  $x = M/R$  can be contrasted with the phenomenological relation  $\tilde{I}(x)$  found in [32]. Considering the cases of the stars with  $M = 1.338M_\odot$ , and  $2M_\odot$  discrepancies of only 1% and 3% have been found respectively. Similar results are obtained by comparing with the formula presented in [16].

The rich structure of the speed of sound is closely related to the symmetry energy of nuclear matter [103], the result of the present model is shown in Fig. 7 in terms of the baryonic density. As already noted in [52], the adiabatic velocity  $v_a$  is continuous but  $v_e$  presents finite discontinuities at the beginning of the coexistence domain, see for instance [104]. Both definitions are almost coincident for low densities. In fact, if the homogenous matter assumption is extended for  $n \rightarrow 0$ , then pure neutron matter is found for  $n < 0.02n_0$  and

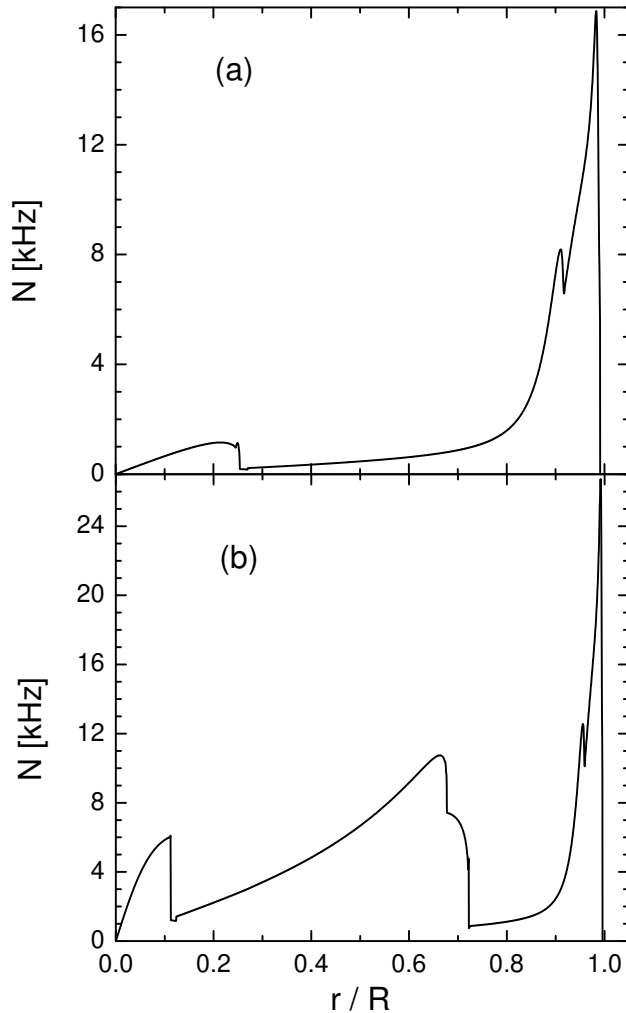


Figure 8: The Brunt-Väisälä frequency as defined by Eq. (16) in terms of the radial coordinate for a star with  $M/M_{\odot} = 1.4$  (a) and  $M/M_{\odot} = 2$  (b), obtained within the F case.

consequently is  $v_e = v_a$  there. A noticeable deviation happens at the onset of the  $\Lambda$  hyperon where  $v_e$  drops suddenly, followed by a continuous increase after the rise of the heavier  $\Xi^-$ . The same kind of structure associated with the presence of the hyperons has been observed in [79, 105]. The conformal limit  $v_{\text{lim}} = c/\sqrt{3}$  is clearly exceeded near the  $\Lambda$  onset, the maximum value obtained for the speed of sound are slightly greater than the proposed upper limit  $v_{\text{max}}/c \geq 0.63$  [106]. Before the deconfinement density is  $v_e/c \simeq 0.69$  and a noticeable fall of roughly 60% is registered after this particular point.

These observations seems to corroborate the relation between the magnitude of the speed of sound and the number  $N$  of effective degrees of freedom. In agreement with the general belief, an increase of  $N$  with the density is locally reflected by a sudden drop in  $v_e$ , which is realized through a finite discontinuity in the case of the phase transition. The growth of  $v_e$  observed between these particular points is consistent with the monotonously increasing trend found in [107], where a variety of nuclear matter equations of state are analyzed.

Closely related to the sound speed is the relativistic Brunt-Väisälä frequency  $N$ , which is shown in Fig. 8 in terms of the radial coordinate for the stars with  $M/M_{\odot} = 1.4$  (a) and 2.0 (b). For the sake of simplicity the assumption of homogeneity is extended to all the range, which leads to  $N = 0$  at the crust

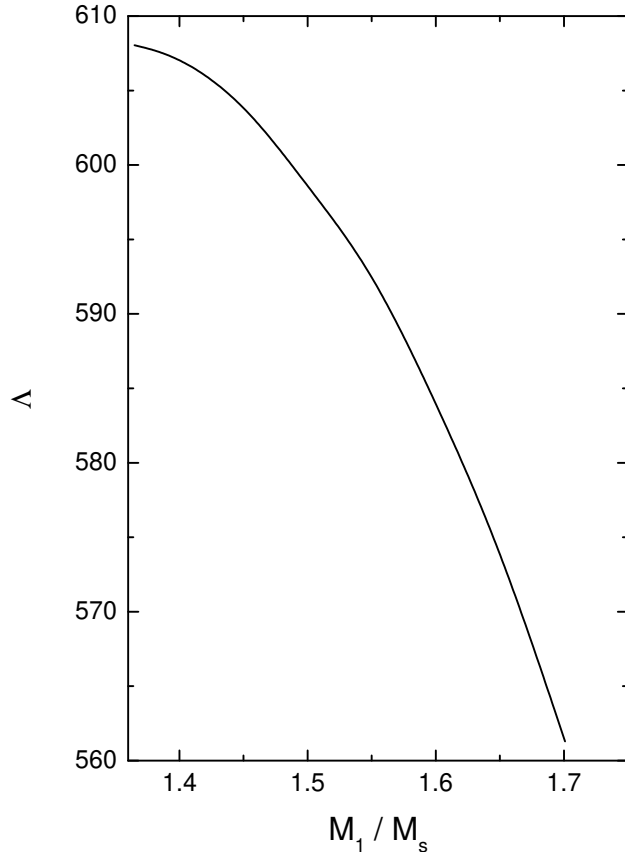


Figure 9: The combined tidal deformability of a binary system (see Eq. (17)) in terms of the mass of the heavier component, as obtained in the F case.

of these stars. The quantity  $N$  is a registry of the bulk properties inside the star, for instance the onset of the muons at the inner crust causes the small irregularity mounted on the left side of the peak at  $r \simeq R$ . At a deeper point one finds a crest corresponding to the onset of the hyperons. It takes place at the core of the star in Fig. 8a, while in Fig. 8b it has a complex structure due to the greater abundance of  $\Lambda$  and  $\Xi^-$  for the heavier star. As already mentioned only a scarce population of  $\Lambda$  appears in the case of  $M/M_\odot = 1.4$ . Finally, a second crest marks the deconfinement and the coexistence of phases at the center of the star shown in Fig. 8b, but it does not occur in Fig. 8a.

The possible value for the tidal deformability of a neutron star with  $M/M_\odot = 1.4$  is within the range  $\Lambda_{1.4} = 190_{-120}^{+390}$ , according to the analysis of [39]. In the present calculations the result  $\Lambda_{1.4} = 527.08$  has been obtained, hence it is compatible with that constraint. It must be pointed out that the star with the canonical mass has, in the present analysis, only a 1% of  $\Lambda$  hyperons in its core. Therefore  $\Lambda_{1.4}$  would not provide information about exotic degrees of freedom. Another parameter of interest is the combined tidal deformability

$$\tilde{\Lambda} = \frac{16}{13} \frac{\Lambda_1 (M_1 + 12 M_2) M_1^4 + \Lambda_2 (M_2 + 12 M_1) M_2^4}{(M_1 + M_2)^5} \quad (17)$$

where  $M_i$ ,  $\Lambda_i$  are the mass and the tidal deformability of the individual components of a binary system. Furthermore the chirp mass, given by the relation

$$\mathcal{M}^5 = \frac{M_1^3 M_2^3}{M_1 + M_2},$$

has been determined with accuracy for the event GW170817 [39], while the possible values for  $M_1$  are expected to range within  $1.3 < M_1/M_\odot < 1.6$ , assuming  $M_2 < M_1$ . Under this constraint I have evaluated  $\tilde{\Lambda}$  in terms of  $M_1$ , as shown in Fig. 9. The result  $560 < \tilde{\Lambda} < 610$  is compatible with the expectations for the low spin prior  $\tilde{\Lambda} \in (70, 800)$  as well for the high spin prior  $\tilde{\Lambda} \in (0, 630)$  [42].

The particular cases of  $\Lambda_{1.4} = 527.05$  and  $\Lambda_{2.01} = 22.2$  have been compared with the predictions of the universal relation proposed in [57] for  $\ln(I/M^3)$  in terms of the tidal deformability. In the first case the discrepancy is negligible and for the more massive case an agreement within 0.1% is found.

The general compatibility with the main phenomenological data on the tidal deformability distinguishes the present treatment in comparison with other models of hyperonic stars [109].

It has been argued that the nonradial oscillation modes of a neutron star can be used to infer structure parameters, such as mass and radius [43], or even they can reveal the high density hadronic EoS [110] and the presence of exotic degrees of freedom [111]. The spectrum of non-radial oscillations for a compact star containing hyperons has been intensively studied [46, 49, 51, 108, 112]. For this reason the fundamental frequency  $\nu_f$  of the f-modes, characterized by the fact that the corresponding radial function  $W(r)$  does not have nodes inside the star, and the highest frequency  $\nu_g$  of the g-mode are examined in the following. The results for these frequencies in terms of the inertial mass are shown in Fig. 10. Both instances, F and N treatments, are considered but only stars within the range of masses allowed by the first case are included. For low  $M$  there is no appreciable difference because such stars have a relatively low central density  $n_c$  and the EoS are practically the same in both cases. But as  $n_c > 2.5n_0$  the presence of hyperons modifies significantly the composition of the core in the F case. Thus the difference becomes apparent for  $M/M_\odot > 1.5$ . The behavior of  $\nu_g$  resembles that found in [52, 56], although in that work the steep growth of the frequency is driven by the deconfinement transition which is effective even for low mass neutron stars. In contrast, I found that only stars with a mass around  $M_{\max}$  have an admixture of hadrons and free quarks in their cores. The common feature with [52, 56] is a sudden rise associated to the Brunt-Väisälä frequency, see Fig. 8, although it has different physical origin.

Recent analysis has estimated the disagreement between the Cowling approximation and the solution of linearized general relativity for  $\nu_g$  is within 10% [56]. In regard of  $\nu_f$ , the comparison between the F and N results is similar to the behavior found in [51] for the  $m^*/m = 0.55$  case. The fitting function given in [51] for the quadrupolar  $l = 2$  component describes our results within the 5% accuracy. Contrary to the expectations the relation for the real angular frequency  $2\pi\nu_f$  in terms of the parameter  $\eta = \sqrt{M^3/I}$  presented in [44], does not describe appropriately our calculations. The cause is twofold: the sampling of models taken in [44] does not include hyperons, therefore a significant discrepancy is expected for high  $M$ . But such cases are precisely the more relevant for the f-mode, since they include the high density regime. And secondly, the use of the relativistic Cowling approximation which induces an error estimated within 30% [55].

The g-modes are sustained by the buoyancy restoration force due to the lack of

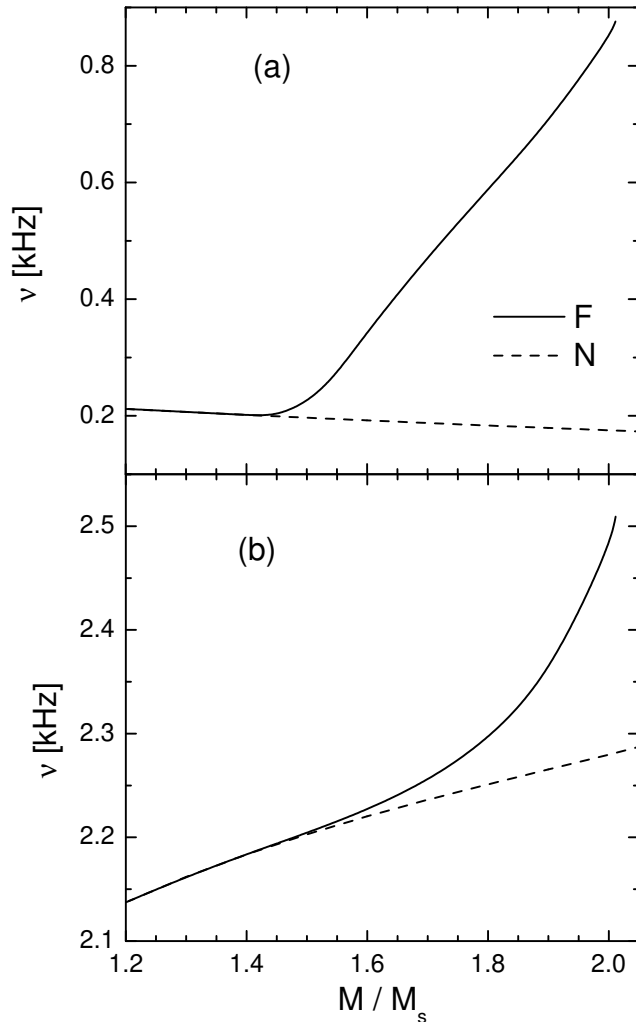


Figure 10: The fundamental frequency of non-radial oscillations for the g-mode (a), and the f-mode (b) as functions of the star mass. The abbreviations F and N are described in the caption of Fig. 1.

chemical homogeneity in a stratified structure. Thus the onset of new degrees of freedom constrained by a chemical potential enlarges the composition gradients and consequently reinforces the frequency  $\nu_g$ . In the F case, such effect could be multiple, to the presence of hyperons in stars with masses  $M/M_\odot > 1.4$ , must be added the onset of deconfined quarks for those with  $M/M_\odot \geq 2$ . For this reason the g-modes have been focused as candidates for revealing the behavior of matter in the deep interior of a star.

It is expected that the g-modes affect the phase of the gravitational wave emitted during the collapse of a binary star system. The underlying mechanism consists in a resonant excitation of the g-modes by the tidal forces in the last stages of the inspiral process. Consequently an energy transfer  $\Delta E$  from the orbital motion to the oscillatory dynamics takes place, modifying the phase of the gravitational waveform. The orbital phase shift  $\Delta\Phi$  due to such mechanism has been estimated in [113]

$$\Delta\Phi \approx \frac{3}{2} \pi \Gamma \left( \frac{\Omega_e(t)}{\pi\nu_g} - 1 \right) \left( -\frac{\Delta E}{E} \right)$$

and used to study the effects of hyperons [114] and quarks [50, 52] in the com-

position of neutron stars. In the preceding equation  $E$ ,  $\Omega_e(t)$  stand for the total orbital energy and the time dependent orbital angular velocity. The same analysis is applied here in order to give a comparative estimation of the effects obtained in the F and N approaches. Neglecting differences in the time evolution of  $\Omega_e(t)/\nu_g$  the following expression is obtained

$$\frac{\Delta\Phi_F}{\Delta\Phi_N} \simeq \left(\frac{\nu_{gN}}{\nu_{gF}}\right)^{1/3} \left(\frac{S_F}{S_N}\right)^2$$

where the overlap integral  $S$  can be evaluated using the functions  $V(r)$ ,  $W(r)$  of the Eqs. 12-14. Taking the case of a star with mass  $M/M_\odot = 1.8$  the quotients  $\nu_{gF}/\nu_{gN} \simeq 3.5$ ,  $S_F/S_N \simeq 1.5$  are obtained, hence  $\Delta\Phi_F \simeq 1.5 \Delta\Phi_N$ . Taking as a reference value the result of [52]  $\Delta\Phi_N \simeq 0.8$ , it is found that  $\Delta\Phi_F \sim \mathcal{O}(1)$ , which means a noticeable correction to the phase shift due to the tidal coupling to the oscillation mode.

The emission of gravitational waves by a pulsating star at a distance  $R$  apart will be distinguishable by a Earth based detector if the energy released  $E_{GW}$  verifies [110]

$$\frac{E_{GW}}{M_\odot} = 3.5 \times 10^{36} \frac{1+4Q^2}{4Q^2} S_n[\text{seg}] \left(\frac{S}{N}\right)^2 R[10 \text{ kpc}]^2 \nu[\text{Khz}]^2$$

where  $S/N$  is the signal to noise ratio,  $S_n$  the spectral density of the detector, and the quality factor of the oscillation is given by  $Q = \pi \nu \tau$ . The damping time of the oscillation  $\tau$  has not been evaluated here, for these reason the range  $10^{-2} \text{ year} \leq \tau \leq 3 \times 10^{-2} \text{ year}$  is considered according to typical values obtained in [50, 115] for a star with  $M/M_\odot = 1.8$ . Adopting the reference values  $S/N = 8$ ,  $S_n = 4 \times 10^{-46} \text{ s}$  [115] corresponding to present LIGO/Virgo characteristics, the results  $E_{GW}^{(N)} \simeq 0.7 \times 10^{46} \text{ erg}$ , and  $E_{GW}^{(F)} \simeq 8 \times 10^{46}$  are obtained for  $R = 10 \text{ kpc}$ . Whereas for  $R = 10 \text{ Mpc}$  the outcomes are  $E_{GW}^{(N)} \simeq 1.6 \times 10^{52} \text{ erg}$ , and  $E_{GW}^{(F)} \simeq 2 \times 10^{53}$ . Since the LIGO/Virgo energy thresholds for detection is about  $10^{46} - 10^{47} \text{ erg}$  for events in our galaxy, and  $10^{52} - 10^{53} \text{ erg}$  for sources in the Virgo cluster, it can be concluded that such illustrative situation is feasible of detection. Furthermore, the relative error in the determination of the frequency has been estimated as [110]

$$\frac{\Delta\nu}{\nu} = 4.2 \times 10^{-3} \frac{R[10 \text{ kpc}]}{\tau[\text{s}]} \sqrt{\frac{1-2Q^2+8Q^4}{4Q^4}} \sqrt{\frac{S_n[10^{-46} \text{ Hz}]}{E_{GW}/M_\odot}}$$

Using this relation, an indetermination of only a few Hz is expected for both N and F cases. Therefore they could be perfectly discernible.

Of course this is a simplified qualitative estimation, a detailed calculation must take into account the statistical error coming from other several parameters of the binary that could affect  $\Delta\Phi$  as well  $\Delta\nu$ .

There is a general belief that hadronic matter at sufficiently high density undergoes a transition to deconfined quark matter. However, the characteristics of such transition are uncertain yet. In this work it is assumed that a preliminary coexistence of phases takes place, which has been interpreted as the consequence of a vanishing interface tension  $\sigma_T$ . At the opposite extreme, for very large  $\sigma_T$ , it is expected a discontinuous transition described by the Maxwell construction. While for intermediate values a non-homogeneous phase would be plausible. These effects have been analyzed in [116] within a specific model, concluding that all of them, the maximum mass, the radius, and the combined tidal

deformability monotonously increase with  $\sigma_T$ . An estimation of the maximum variation due to finite tension is given there as  $\Delta M_{\max}/M_{\odot} = 0.02$ ,  $\Delta R = 0.6$  km, and  $\Delta\tilde{\Lambda}/\tilde{\Lambda} = 0.5$  [116]. Thus a scarce increase in the maximum mass can be obtained at the cost of a small growth of the radius and a considerable increment of the tidal deformability.

The details of the composition of extreme density matter are still speculative, although they can be a determining factor for the structure of compact stars. Different hypothesis has been explored, as for instance superconducting quark matter, giving rise to a variety of effective theoretical models. This uncertainty is evidenced by the amplitude of values assigned to certain model parameters such as the quark-quark coupling constant or the energy gap between normal and paired states. A large number of studies have discussed the effects of superconducting quark matter have on the properties of compact stars [117, 118, 119, 120, 121]. For instance in [117] an effective nuclear model is used in combination with a bag model including a color-flavor locked superconducting phase. For the latter model the parameters are taken as  $B = 137$  MeV/fm<sup>3</sup>,  $m_s = 200$  MeV and  $\Delta = 100$  MeV for the energy gap. The mass-radius relation for the neutron star shows the significant fact that a sharp quark-hadron phase transition leads to a unstable star structure. In contrast, the continuous phase transition allows the existence of stable configurations with unbound quarks. In any case the maximum mass is slightly reduced as compared with the unpaired case. This behavior is qualitatively confirmed in [118] where the dynamics of the deconfined quarks is determined by the NJL within two different parametrizations. Since the quark-quark interaction is unknown, the authors assume the same coupling constant as in the four fields quark-antiquark interaction  $G_D = G$ . They only consider a sharp hadron-quark phase transition and also include the possibility of light quark superconducting phase (2SC), with unpaired strange flavor, in addition to the just mentioned color-flavor locked arrangement. In this case, the presence of the intermediate two-flavor pairing introduces a narrow window of stability before the color-flavor locked phase becomes preferable.

These type of instabilities have been related to the lack of confinement of the NJL model [122], and attributed to the zero energy point  $\mathcal{E}_0$ . This argument has been examined in [120], where a different procedure to fix the additive constant has been proposed. With this modified constant  $\mathcal{E}_0^*$ , an intermediate stable 2SC phase was found, as in [118]. A further increase of the pairing coupling constant to  $G_D = 1.2G$ , in combination with  $\mathcal{E}_0^*$ , extends the range of stability to embrace the color-flavor locked phase. At the same time the allowed maximum mass for neutron stars is reduced [120].

Based on this results one can conclude that the inclusion of a superconducting quark phase, if stable, will lead to a decrease of  $M_{\max}$ .

## 5 Summary and Conclusions

This work is devoted to the study of dense matter at zero temperature, as can be found in the interior of neutron stars. For this purpose a composite model of the strong interaction is used. In the low density limit a nonhomogeneous phase including light atomic nuclei is considered through the standard results of [80]. For higher densities a model of the field theory including hyperons is used to describe a homogeneous hadronic phase. For the extreme densities fea-



sible in the core of a compact star, a phase of deconfined quarks is taken into account through the NJL model with vector current-current coupling. In between a coexistence of hadronic and free quark phases is assumed, which allows a continuous variation of the thermodynamic potential.

The role of hyperons is particularly analyzed in the context of the “hyperon puzzle”. Thus an extension of a previously defined hadronic model [86, 79] is made by including hyperon-hyperon interaction mediated by the  $a_0(980)$  and hidden strangeness  $f_0(980)$  mesons. In order to emphasize the hyperonic effects a complementary scheme, which only considers nucleons and leptons, is introduced.

Several properties of a static or slowly rotating neutron star has been evaluated, such as maximum mass, moment of inertia, tidal deformability, etc., and contrasted with recent observational data or with different universal relations. Since the nature of the compact object with mass  $M/M_\odot \simeq 2.6$  detected by [4] is still uncertain, it is not actively considered here. The confirmation that it is a neutron star would put most of the present models of the strong interaction satisfying explicit relativistic covariance and agreement with other observational data in conflict.

Within this approach only stars with masses  $M/M_\odot \geq 1.45$  show clear evidence of the presence of hyperons, and only those with  $M/M_\odot \simeq 2$  have a trace of deconfined quarks in their cores.

The pressure at a density twice the normal nuclear density is coherent with the estimations based on the data obtained in the GW170817 event [39]. The mass-radius relation for the maximum mass predicted in the present treatment  $M/M_\odot = 2.01$ ,  $R = 11.7$  km is within the confidence range proposed for the PSR J0740+6620 [23].

The imminent high precision measurement of the moment of inertia of the PSR J0737-3039A has motivated intense work. Focusing on a star with the same mass, our result for the moment of inertia is compatible with different predictions [16, 35].

Focusing on a star with the canonical mass  $M/M_\odot = 1.4$ , I found its radius is in agreement with the analysis in [24, 102]. Furthermore, its tidal deformability  $\Lambda_{1.4}$  verifies the constraint  $\Lambda_{1/4} < 580$  established in [39]. Considering a binary system with chirp mass  $\mathcal{M}/M_\odot = 1.186$  the result for the combined tidal deformability verifies  $566 < \Lambda < 608$  which is compatible with the observational evidence [42].

The calculations for the frequencies  $\nu$  of the nonradial f and g-modes for a neutron star are qualitatively similar to previous results for either including hyperons (F) or considering only nucleons and leptons (N). The Brunt-Väisälä frequency have peaks associated with the onset of the hyperons similar to those found for the deconfinement transition [52]. They are the cause of important deviations of the frequencies found in the F case as compared with the N treatment. This is a confirmation of previous findings for  $\nu_g$  [52] as well as for  $\nu_f$  [51].

In addition, positive confirmations of our results are obtained when contrasting with the universal relations proposed for the moment of inertia in terms of the compactness [16, 32], the tidal deformability as a function of the moment of inertia [57], and the f-mode frequency in terms of  $M/R^3$  [51].

In summary, the model used here requires only a concise set of parameters inspired on basic phenomenological grounds and its predictions are in good agreement with a variety of recent observational data as well as phenomenological relations on neutron stars. Hence one can conclude that the presence

of hyperons and a deconfinement transition are compatible with the present knowledge on compact stars.

## Acknowledgements

This work was partially supported by the CONICET, Argentina under grant PIP-616.

## References

- [1] Demorest P. B., Pennucci T., Ransom S. M., Roberts M. S. E., and Hessels J. W. T. 2010 *Nature* **467** 1081.
- [2] Romani R. W., Kandel D., Filippenko A. V., Brink T. G., and Zheng W. K. 2021 *Astroph. J. Lett.* **908** L46; 2022 *Astroph. J. Lett.* **934** L18.
- [3] Fonseca E. et al. 2021 *Astroph. J. Lett.* **915** L12.
- [4] Abbott R. et al. 2020 *Astroph. J. Lett.* **896** L44.
- [5] Fattoyev F. J., Horowitz C.J., Piekarewicz J., Reed B. T. 2020 *Phys. Rev. C* **102** 065805.
- [6] Bednarek I., Haensel P., Zdunik J. L., Beiger M., Manka R. 2012 *Astron. Astroph.* **543** 157
- [7] Lim Y., Lee C.-H., Oh Y. 2018 *Phys. Rev. D* **97** 023010.
- [8] Burgio G. F., Schulze H.-J., Vidaña I., Wei J.-B. 2021 *Prog. Part. Nuc. Phys.* **120** (2021) 103879.
- [9] Cai B.-J., Fattoyev F. J., Li B.-A., Newton W. G. 2015 *Phys. Rev. C* **92** 015802.
- [10] Sahoo H. S., Mitra G., Mishra R., Panda P. K., Li B.-A. 2018 *Phys. Rev. C* **98** 045801.
- [11] Sun T.-T., Zhang S.-S., Zhang Q.-L., Xia C.-J. 2019 *Phys. Rev. D* **99** 023004.
- [12] Ribes P., Ramos A., Tolos L., Gonzalez-Boquera C., Centelles M. 2019 *Astroph. J.* **883** (2019) 168.
- [13] Sen D. 2021 *Phys. Rev. C* **103** 045804.
- [14] Marczenko M., Redlich K., Sasaki C. 2022 *Phys. Rev. D* **105** (2022) 103009.
- [15] Shao G.-y., Liu Y.-x. 2010 *Phys. Rev. C* **82** 055801.
- [16] Lim Y., Kwak K., Hyun C. H., Lee C.-H. 2014 *Phys. Rev. C* **89** 055804.
- [17] Thapa V. B., Sinha M. 2020 *Phys. Rev. D* **102** 123007.
- [18] Paoli M. G., Menezes D. P. 2010 *Eur. Phys. J. A* **46** 413.
- [19] Ellis J., Hutsi G., Kannike K., Marzola L., Raidal M., Vaskonen V. 2018 *Phys. Rev. D* **97** 123007.

- [20] Das H. C., Kumar A., Patra S. K. 2021 Phys. Rev. D **104** 063028.
- [21] Leung K.-L., Chu M.-c., Lin L.-M. 2022 Phys. Rev. D **105** (2022) 123010.
- [22] Riley T. E. et al. 2017 Astroph. J. Lett. **887** L21.
- [23] Riley T. E. et al. 2021 Astroph. J. Lett. **918** L27.
- [24] Raijmakers G. et al. 2021 Astroph. J. L. **918** L29.
- [25] Müller H., Serot B. D. 1996 Nuc. Phys. A **606** 508.
- [26] Lalazissis G. A., Konig J., Ring P. 1997 Phys. Rev. C **55** 540.
- [27] Das A., Malik T., Nayak A. C. 2019 Phys. Rev. D. **99** 043016.
- [28] Das H. C., Kumar A., Patra S. K. 2021 Phys. Rev. D. **104** 063028.
- [29] Newton W. G., Steiner A. W., Yagi K. 2018 Astroph. J. **856** 19.
- [30] Lyne A. G. et al. 2004 Science **303** 1153.
- [31] Morrison I. A., Baumgarte T. W., Shapiro S. L., Pandharipande V. R. 2004 Astroph. J. **617** L135.
- [32] Lattimer J. M., Schutz B. F. 2005 Astroph. J. **629** 979.
- [33] Raithel C. A., Ozel F., Psaltis D. 2016 Phys. Rev. C. **93** 032801(R).
- [34] Greif S. K., Hebeler K., Lattimer J. M., Pethick C. J., Schwenk A. 2020 Astroph. J. **901** 155.
- [35] Landry P., Kumar B. 2018 Astroph. J. L. **868** L22.
- [36] Lim Y., Holt J. W., Stahulak R. J. 2019 Phys. Rev. C. **100** 035802.
- [37] Hinderer T. 2008 Astroph. J. **677** 1216.
- [38] Abbott B. P. et. al. 2017 Phys. Rev. Lett. **119** 161101.
- [39] Abbott B. P. et. al. 2018 Phys. Rev. Lett. **121** 161101.
- [40] Thorne K. S., Campolattaro A. 1967 Astroph. J. **149** 591.
- [41] McDermott P. N., Van Horn H. M., Scholl J. F. 1983 Astroph. J. **268** 837.
- [42] Abbott B. P. et. al. 2019 Phys. Rev. X **9** (2019) 011001.
- [43] Andersson N., Kokkotas K. D. 1998 Mon. Not. R. Astron. Soc. **299** 1059.
- [44] Lau H. K., Leung P. T., Lin L. M. 2010 Astroph. J. **714** 1234.
- [45] Wen D.-H., Li B.-A., Chen H.-Y., Zhang N.-B. 2019 Phys. Rev. C **99** 045806.
- [46] Sotani H., Kumar B. 2021 Phys. Rev. D **104** 123002.
- [47] Chirenti C., de Souza G. H., Kastaun W. 2015 Phys. Rev. D **91** 044034.
- [48] Sotani H., Yasutake N., Maruyama T., Tatsumi T. 2011 Phys. Rev. D **83** 024014.

- [49] Blazquez-Salcedo J. L., Gonzalez-Romero L. M., Navarro-Lerida F. 2014 Phys. Rev. D **89** 044006.
- [50] Wei W., Salinas M., Klahn T., Jaikumar P., Barry M. 2020 Astroph. J. **904** 187.
- [51] Pradhan B. K., Chatterjee D. 2021 Phys. Rev. C **103** 035810; Pradhan B. K., Pathak D., Chatterjee D. 2023 Astroph. J. **956** 38.
- [52] Jaikumar P., Semposki A., Prakash M., Constantinou C. 2021 Phys. Rev. D **103** 123009.
- [53] Constantinou C., Han S., Jaikumar P., Prakash M. 2021 Phys. Rev. D **104** 123032.
- [54] Das H. C., Kumar A., Biswal S. K., Patra S. K. 2021 Phys. Rev. D **104** 123006.
- [55] Kunjipurayil A., Zhao T., Kumar B., Agrawal B. K., Prakash M. 2022 Phys. Rev. D **106** 063005.
- [56] Zhao T., Constantinou C., Jaikumar P., Prakash M. 2022 Phys. Rev. D **105** 103025.
- [57] Yagi K., Yunes N. 2013 Phys. Rev. D **88** 023009.
- [58] Kumar B., Landry P. 2019 Phys. Rev. D **99** 123026.
- [59] Takami K., Rezzolla L., Baiotti L. 2014 Phys. Rev. Lett. **113** 091104.
- [60] Most E. R., Weih L. R., Rezzolla L., Schaffner-Bielich J. 2018 Phys. Rev. Lett. **120** 261103.
- [61] Nandi R., Char P., Pal S. 2019 Phys. Rev. C **99** 052802(R).
- [62] Lourenco O., Dutra M., Lenzi C. H., Flores C. V., Menezes D. P. 2019 Phys. Rev. C **99** 045202.
- [63] Li J. J., Sedrakian A. 2019 Astroph. J. lett. **874** l22.
- [64] Traversi S., Char P., Pagliara G. 2020 Astroph. J. **897** 165.
- [65] Gomes R. O., Char P., Schramm S. 2019 Astroph. J. **877** 139.
- [66] Han S., Mamun M. A. A., Lalit S., Constantinou C., Prakash M. 2019 Phys. Rev. D **100** 103022.
- [67] Dexheimer V., Gomes R. O., Schramm S., Pais H. 2019 J. Phys. G **46** 034002.
- [68] Landry P., Essick R., Chatziioannou K. 2020 Phys. Rev. D **101** 123007.
- [69] Essick R., Landry P., Holz D. E. 2020 Phys. Rev. D **101** 063007.
- [70] Essick R., Tews I., Landry P., Reddy S., Holz D. E. 2020 Phys. Rev. C **102** 055803.  
Essick R., Tews I., Landry P., Schwenk A. 2021 Phys. Rev. Lett. **127** 192701.  
Essick R., Landry P., Schwenk A., Tews I. 2021 Phys. Rev. C **104** 065804.

- [71] Reed B. T., Fattoyev F. J., Horowitz C.J., Piekarewicz J. 2021 Phys. Rev. Lett. **126** 172503.
- [72] Blacker S., Bastian N.-U. F., Bauswein A., Blaschke D. B., Fischer T., Oertel M., Sultanis T., Typel S. 2020 Phys. Rev. D **102** (2020) 123023.
- [73] Lau S. Y., Yagi K. 2021 Phys. Rev. D **103** 063015.
- [74] Legred I., Chatziioannou K., Essick R., Han S., Landry P. 2021 Phys. Rev. D **104** 063003.
- [75] Pang P. T. H. et al. 2021 Astroph. J. **922** 14.
- [76] Most E. R., Papenfort L. J., Dexheimer V., Hanauske M., Schramm S., Stocker H., Rezzolla L. 2019 Phys. Rev. Lett. **122** 061101.  
Most E. R., Papenfort L. J., Dexheimer V., Hanauske M., Stoecker H., Rezzolla L. 2020 Eur. Phys. J. A **56** 59.
- [77] Ferreira M., Providencia C. 2021 Phys. Rev. D **104** 063006.
- [78] Shangguan W. Z., Huang Z. Q., Wei S. N., Jiang W. Z. 2021 Phys. Rev. D **104** 063035.
- [79] Aguirre R. M. 2022 Phys. Rev. D **105** 116023.
- [80] Baym G., Pethick C., Sutherland P. 1971 Astroph. J. **170** 299.
- [81] Glendenning N. K. 1985 Astroph. J. **293** 470.
- [82] Serot B. D., Walecka J. D. 1997 Int. J. Mod. Phys. E **6** 515.
- [83] Boguta J., Bodmer A. R. 1977 Nucl. Phys. A **292** 413.
- [84] Horowitz C. J., Piekarewicz J. 2000 Phys. Rev. Lett. **86** 5647.
- [85] Fattoyev F. J., Horowitz C. J., Piekarewicz J., Shen G. 2010 Phys. Rev. C **82** 055803.
- [86] Miyatsu T., Cheoun M.-K., Saito K. 2022 Astrophys. J. **929** 82.
- [87] Kubis S., Wojcik W., Zabari N. 2020 Phys. Rev. C **102** 065803.
- [88] Schaffner J., Dover C. B., Gal A., Greiner C., Millener D. J., Stocker H. 1994 Ann. Phys. **235** 35.
- [89] Vidaña I., Polls A., Ramos A., Schulze H.-J. 2011 Phys. Rev. C **64** 044301.
- [90] Gal A., Hungerford E. V., Millener D. J. 2016 Rev. Mod. Phys. **88** 035004.
- [91] Oertel M., Providencia C., Gulminelli F., Raduta Ad. R. 2015 J. Phys. G **42** 075202.
- [92] Torres J. R., Gulminelli F., Menezes D. P. 2017 Phys. Rev. C **95** 025201.
- [93] Li J. J., Long W. H., Sedrakian A. 2018 Eur. Phys. J. A **54** 133.
- [94] Klevansky S. P. 1999 Rev. Mod. Phys. **64** 649.
- [95] Rehberg P., Klevansky S. P., Hufner J. 1996 Phys. Rev. C **53** 410.
- [96] Hartle J. B. 1967 Astroph. J. **150** 1005.

- [97] Yoshida S., Eriguchi Y. 1997 *Astrophys. J.* **490** 779.
- [98] Yoshida S., Kojima Y. 1997 *Mon. Not. Roy. Astron. Soc.* **289** 117.
- [99] Sotani H., Takiwaki T. 2020 *Phys. Rev. D* **102** 063025.
- [100] Yang F., Shen H. 2008 *Phys. Rev. C* **77** 025801.
- [101] Zhang N.-B., Li B.-A. 2021 *Astroph. J.* **921** 111.
- [102] Miller M. C. et al. 2021 *Astroph. J. Lett.* **918** L28.
- [103] Zhang N.-B., Li B.-A. 2023 *Eur. Phys. J. A* **59** 86.
- [104] Pal S., Podder S., Sen D., Chaudhuri G. 2023 *Phys. Rev. D* **107** 063019.
- [105] Motta T. F., Guichon P. A. M., Thomas A. W. 2021 *Nucl. Phys. A* **1009** 122157.
- [106] Alsing J., Silva H. O., Berti E. 2018 *Mont. Not. Roy. Astron. Soc.* **478** 1377.
- [107] Moustakidis Ch. C., Gaitanos T., Margaritis Ch., Lalazissis G. A. 2017 *Phys. Rev. C* **95** 045801.
- [108] Kumar D., Mishra H., Malik T. 2023 *JCAP* **02** 015.
- [109] Fortin M., Raduta A. R., Avancini S., Providencia C. 2020 *Phys. Rev. D* **101** 034017.
- [110] Kokkotas K. D., Apostolatos T. A., Andersson N. 2001 *Mon. Not. R. Astron. Soc.* **320** 307.
- [111] Sotani H., Tominaga K., Maeda K. I. 2001 *Phys. Rev. D* **65** 024010.
- [112] Benhar O., Ferrari V., Gualtieri L. 2004 *Phys. Rev. D* **70** 124015; Benhar O. 2005 *Mod. Phys. Lett. A* **20** 2335; Chatterjee D., Bandhyopadhyay D. 2009 *Phys. Rev. D* **80** 023011; Lin W., Li B.-A., Xu J., Ko C. M., Wen D. H. 2011 *Phys. Rev. C* **83** 045802; Blazquez-Salcedo J. L., Gonzalez-Romero L. M., Navarro-Lerida F. 2013 *Phys. Rev. D* **87** 104042; Pradhan B. K., Chatterjee D., Lanoye M., Jaikumar P. 2022 *Phys. Rev. C* **106** 015805; Thapa V. B., Beznogov M. V., Raduta A. R., Thakur P. 2023 *Phys. Rev. D* **107** 103054; Tran V., Ghosh S., Lozano N., Chatterjee D., Jaikumar P. 2023 *Phys. Rev. C* **108** 015803.
- [113] Reisenegger A., Goldreich P. 1994 *Astroph. J.* **426** 668.
- [114] Yu, H, Weinberg N. N. 2017, *Montl. Not. Roy. Astron. Soc.* **470** 350.
- [115] Zheng Z.-Y., Sun T. T., Chen H., Wei J.-B., Burgio G. F., Schulze H.-J. 2023 *Phys. Rev. D* **107** 103048.
- [116] Xia C. J., Maruyama T., Yasutake N., Tatsumi T. 2019 *Phys. Rev. D* **99** 103017.
- [117] Alford M. and Reddy S. 2003 *Phys. Rev. D* **67** 074024.
- [118] Buballa M., Neumann F., Oertel M., Shovkovy I. 2004 *Phys. Lett. B* **595** 36.

- [119] Lawley S., Bentz W., Thomas A. W. 2006 J. Phys. G **32** 667.
- [120] Pagliara G., Schaffner-Bielich J. 2008 Phys. Rev. D **77** 063004.
- [121] Paulucci I., Ferrer E. J., Horvath J. E., de la Incera V. 2013 J. Phys. G **40** 125202.
- [122] Baldo M., Burgio G. F., Castorina P., Plumari S., Zappala D. 2007 Phys. Rev. C **75** 035804.